Hindawi
Advances in Mathematical Physics
Volume 2022, Article ID 5635514, 12 pages
https://doi.org/10.1155/2022/5635514

Research Article

Regarding on the Results for the Fractional Clannish Random Walker's Parabolic Equation and the Nonlinear Fractional Cahn-Allen Equation

Md. Nur Alam,[1] **Onur Alp İlhan**,[2] **Md. Sabur Uddin**,[1,3] **and Md. Abdur Rahim**[4]

[1]*Department of Mathematics, Pabna University of Science & Technology, Pabna-6600, Bangladesh*
[2]*Faculty of Education, Erciyes University, 38039-Melikgazi-Kayseri, Turkey*
[3]*Department of Applied Mathematics, Gono Bishwabidyalay, Savar, Dhaka-1344, Bangladesh*
[4]*Department of Computer Science and Engineering, Pabna University of Science and Technology, Pabna-6600, Bangladesh*

Correspondence should be addressed to Md. Nur Alam; nuralam.pstu23@gmail.com

Received 27 December 2021; Accepted 29 March 2022; Published 18 April 2022

Academic Editor: Eugen Radu

In this research, the (Ψ, Φ)-expansion scheme has been implemented for the exact solutions of the fractional Clannish Random Walker's parabolic (FCRWP) equation and the nonlinear fractional Cahn-Allen (NFCA) equation. Some new solutions of the FCRWP equation and the NFCA equation have been obtained by using this method. The diverse variety of exact outcomes such as intersection between rough wave and kinky soliton wave profiles, intersection between lump wave and kinky soliton wave profiles, soliton wave profiles, kink wave profiles, intersection between lump wave and periodic wave profiles, intersection between rough wave and periodic wave profiles, periodic wave profiles, and kink wave profiles are taken. Comparing our developed answers and that got in previously written research papers presents the novelty of our investigation. The above techniques could also be employed to get exact solutions for other fractional nonlinear models in physics, applied mathematics, and engineering.

1. Introduction

Nonlinear fractional mathematical models (NLFMMs) are broadly implemented to express lots of significant phenomena and nonlinear dynamic applications in applied mathematics, mathematical physics, engineering, signal processing, electromagnetics, communications, acoustics, genetic algorithms, viscoelasticity, robotics, electrochemistry, transport systems, material science, finance, image processing, stochastic dynamical systems, biology, plasma physics, chemistry, nonlinear control theory, and so many. In accordance with determining the exact answers of NLFMMs, countless influential and well-organized schemes have been presented and industrialized, such as the variation of (G'/G)-expansion scheme [1], modified (G'/G)-expansion technique [2–5], the first integral technique [6], generalized Kudryashov technique [7], fractional subequation scheme [8, 9], improved fractional sub-equation scheme [10], generalized exponential rational task scheme [11], novel extended direct algebraic method [12], Sine-Gordon expansion technique [13], subequation scheme [14], Kudryashov technique [15], Jacobi elliptic task scheme [16], exp-task scheme [17], the Jacobi elliptic ansatz method [18], natural transform method [19], fractional iteration algorithm [20, 21], the unified method [22], the hyperbolic and exponential ansatz method [23], $(1/G')$-expansion scheme [24], modified decomposition method [25], the quintic B-spline approaches [26], an efficient semi-analytical algorithm [27], the Jacobi elliptic function expansion (JEFE) method [28], the Lie symmetry technique [29], Hirota's simple method [30, 31], the modified extended tanh expansion method [32], exponential finite difference method

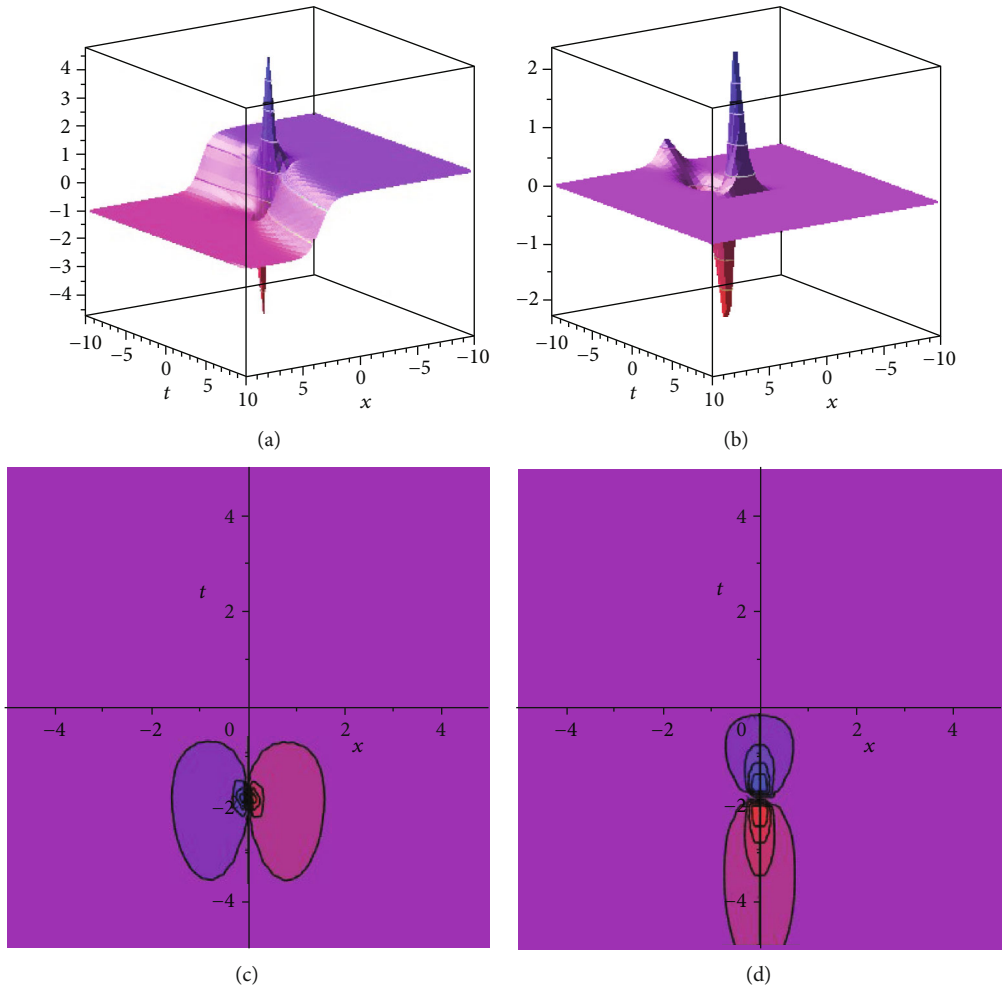

FIGURE 1: The graphical representation of the solution $\lambda_1(x,t)$: (a) real three-dimensional shape, (b) complex three-dimensional shape, (c) real contour plot, and (d) imaginary contour plot.

[33], and many more. Currently, Shehata and Amra [34] discovered a profoundly significant enlargement of the (G'/G) -extension process, called the variation of (G'/G)-expansion process to secure exact solutions of fractional nonlinear models. We instrument the variation of (G'/G)-expansion way for making exact answers to the fractional nonlinear models in the existing effort to express the suitable and simplicity of the process. Therefore, we can effortlessly exchange the fractional nonlinear models into NPDE or NODE via appropriate conversion, with the purpose of everybody acquainted with fractional calculus lacking any trouble. The chief advantage of the process implemented in this study over the other scheme is that it contributes additional novel exact answers, including added independent parameters, and we make a few novel results as well. The exact answers have vast significance in uncovering the fundamental device of the physical events. Apart from the dynamic relevance, the exact answers of fractional nonlinear models support the numerical solvers to compare their results' accuracy and help them in the stability analysis. In our current effort, we instrument (Ψ, Φ)-expansion scheme for constructing exact answers of FCRWP and NFCA equations. We can therefore easily convert FCRWP and NFCA equations into nonlinear PDE or ODE via appropriate conversion, with the purpose of everybody acquainted with fractional calculus lacking any trouble.

In the current object, the first subdivision offers the choice of the research as an introduction. The second subdivision covers a few analyze of the (Ψ, Φ)-expansion method. In the third subdivision, we will acquire answers of the FCRWP and NFCA equations by using the proposed technique. In the fourth subdivision, we will give some numerical simulation of the results obtained. In the last subdivision, we implement the conclusion.

2. Overview of the Technique

In this part of the study, detailed information on fractional calculus theory can be found at [35–37]. Here, we briefly analyzed the modified Lehman-Liouville derivative (MRLD) from the current fractional calculus recommended through Jumarie [38, 39] and provided a research

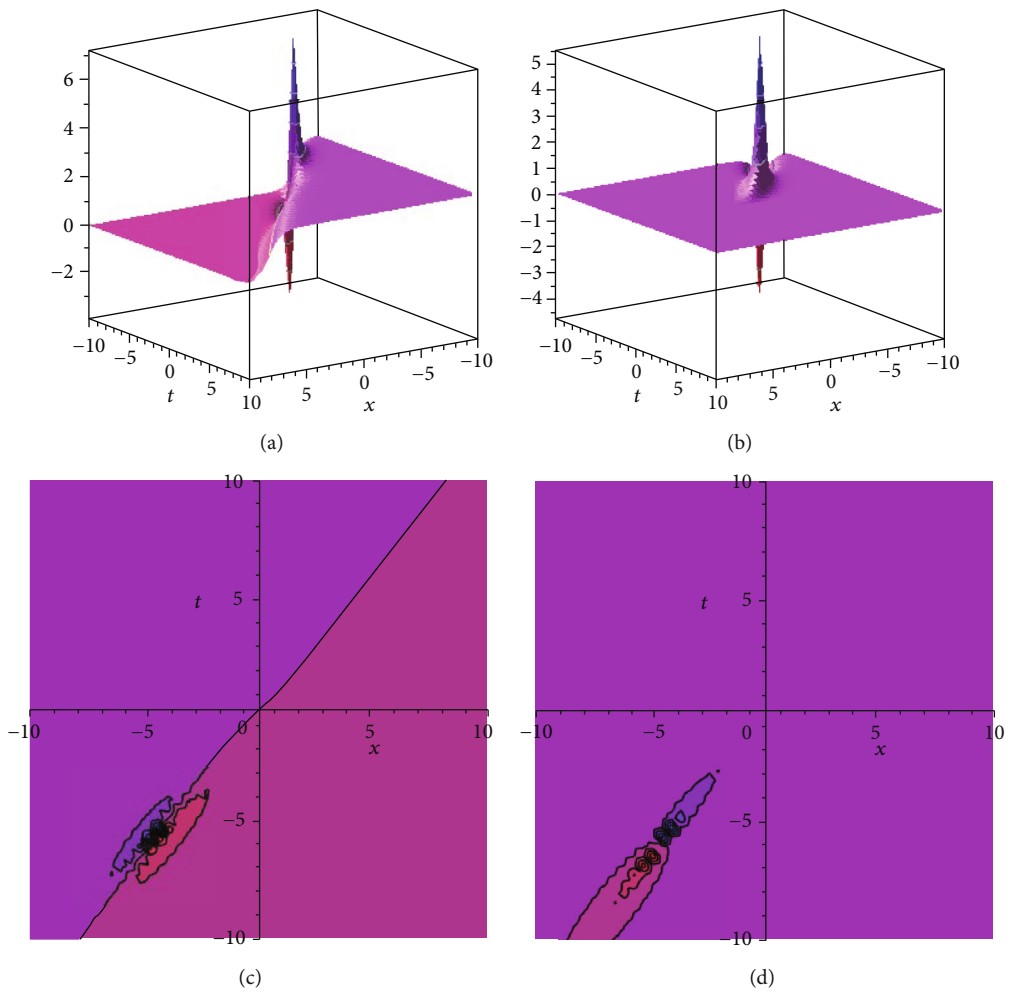

FIGURE 2: The graphical representation of the solution $\lambda_3(x,t)$: (a) real three-dimensional shape, (b) complex three-dimensional shape, (c) real contour plot, and (d) imaginary contour plot.

method. Let $S:[0,1]\longrightarrow \Re$ be a continuous function and $\beta\in(0,1)$. Jumarie has improved the fractional derivative of the order β and S could be clearly defined through [40] as

$$D_{\lambda}^{\beta}S(\lambda)=\begin{cases}\dfrac{1}{\Gamma(-\beta)}\displaystyle\int_0^{\lambda}(\lambda-\chi)^{-\beta-1}[S(\chi)-S(0)]d\chi, & 0>\beta,\\ \dfrac{1}{\Gamma(1-\beta)}\dfrac{d}{dx}\displaystyle\int_0^{\lambda}(\lambda-\chi)^{-\beta}[S(\chi)-S(0)]d\chi, & 0<\beta<1,\\ \left(S^{(n)}(\lambda)\right)^{(\beta-n)}, & n\le\beta\le n+1,\ n\ge 1.\end{cases}\tag{1}$$

We consider

$$P(\lambda,\lambda_x,\lambda_{xx},\lambda_t,\lambda_{tt},\lambda_{xt}.,\cdots..)=0,\tag{2}$$

where P is a polynomial in λ as well as its derivatives. First, use the travelling variable:

$$\lambda=\lambda(x,t)=\lambda(\chi),\chi=p_3(x-Vt),\tag{3}$$

where p_3 and V are a constant to be determined later. Using (3) into (2), We get the following ordinary differential equation:

$$R\left(\lambda,p_3\lambda',p_3^2\lambda'',-p_3V\lambda',p_3^2V^2\lambda'',-p_3^2V^2\lambda'',\cdots..\right)=0.\tag{4}$$

Second, considering the solving form:

$$\lambda(\chi)=\sum_{i=0}^{M}S_i\Psi^i+\sum_{i=1}^{M}T_i\Psi^{i-1}\Phi,\tag{5}$$

where $\Psi=(\Theta'/\Theta)$, $\Phi=(\Omega'/\Omega)$, and $\Theta=\Theta(\chi)$, $\Omega=\Omega(\chi)$ represent as

$$\Theta'(\chi)=-\Theta(\chi)\Omega(\chi),\quad \Omega'(\chi)=1-\Omega(\chi)^2,\tag{6}$$

The above equations provide as follows:

$$\Theta(\chi)=\pm\sec h(\chi),\quad \Omega(\chi)=\tanh(\chi),\tag{7}$$

$$\Theta(\chi)=\pm\csc h(\chi),\quad \Omega(\chi)=\coth(\chi).\tag{8}$$

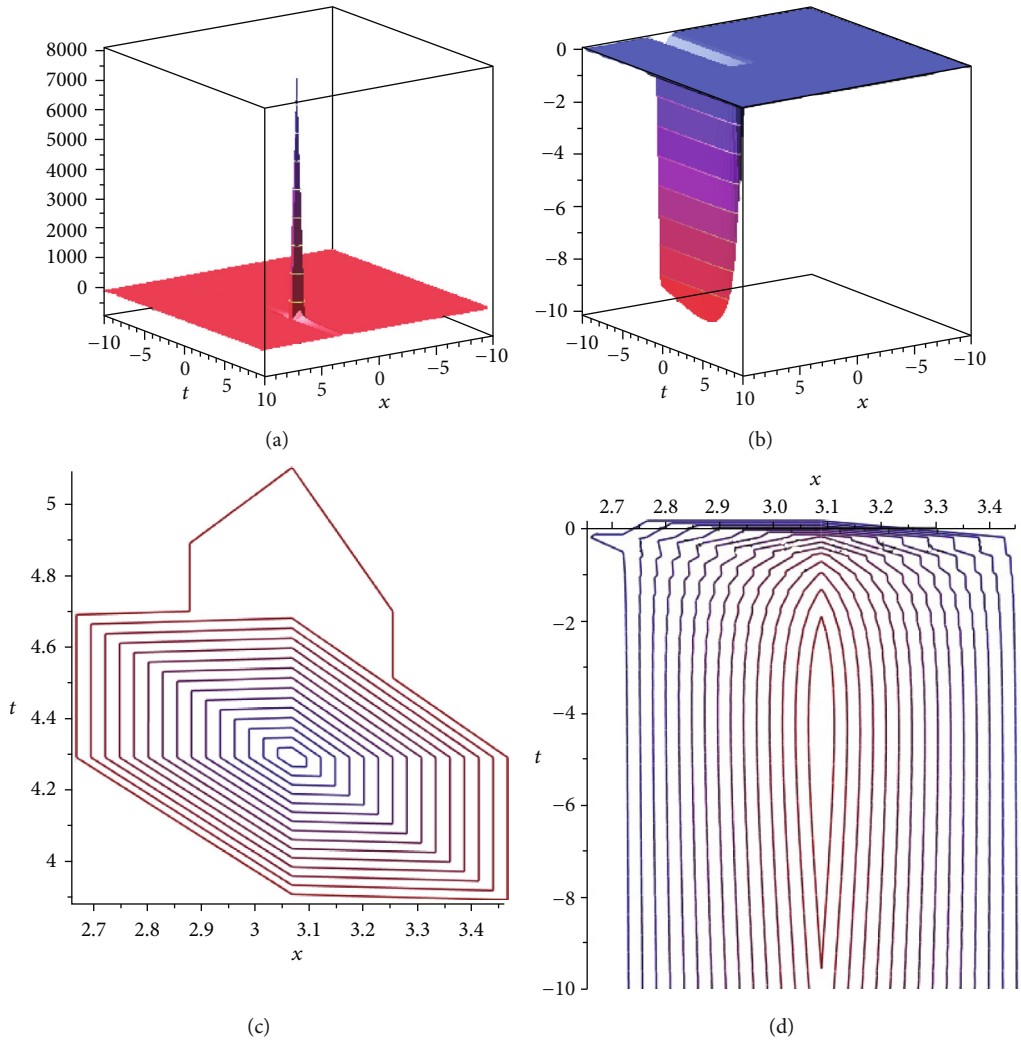

FIGURE 3: The graphical representation of the solution $\lambda_6(x,t)$: (a) real three-dimensional shape, (b) complex three-dimensional shape, (c) real contour plot, and (d) imaginary contour plot.

Third, a polynomial in Ψ or Φ accomplished plugging equation (5) into equation (4). Defining the constant values of the corresponding power of Ψor Φ yields a system of equations, which might be defined to make S_i and T_i. After getting S_i and T_i in (5), the answers of the studied model complete the intention of the answers of the proposed model.

3. Mathematical Analysis

This section presents solutions of two NLFMMs via the (Ψ, Φ) -expansion technique.

3.1. Constructing the Solutions of the FCRWP Equation. We are considering the FCRWP equation [41].

$$\frac{\partial^{\beta}\lambda}{\partial t^{\beta}} - \frac{\partial\lambda}{\partial x} + 2\lambda\frac{\partial\lambda}{\partial x} + \frac{\partial^{2}\lambda}{\partial x^{2}} = 0, t > 0, 0 < \beta, \tag{9}$$

With $\lambda(x,0) = S(x)$. By getting the variable $(x,t) = \lambda(\chi)$, $\chi = x - Vt^{\beta}/\Gamma(\beta+1)$ in equation (9), then, we have

$$-V\lambda' - \lambda' + 2\lambda\lambda' - \lambda'' = 0. \tag{10}$$

The pole of equation (10) is set $N = 1$. Then, we find from equation (4)

$$\lambda(\chi) = S_0\Psi^0 + S_1\Psi^1 + T_1\Psi^0\Phi = S_0 + \frac{T_1}{\Omega} - (S_1 + T_1). \tag{11}$$

Assembling the coefficient of and solving the resulting system, then, we find

Cluster I:

$$V = V, S_0 = 0, S_1 = S_1, T_1 = 0. \tag{12}$$

Substituting the above values in equation (11), we get

$$\lambda_1(x,t) = -S_1 \tanh\left\{x - \frac{Vt^{\beta}}{\Gamma(\beta+1)}\right\}. \tag{13}$$

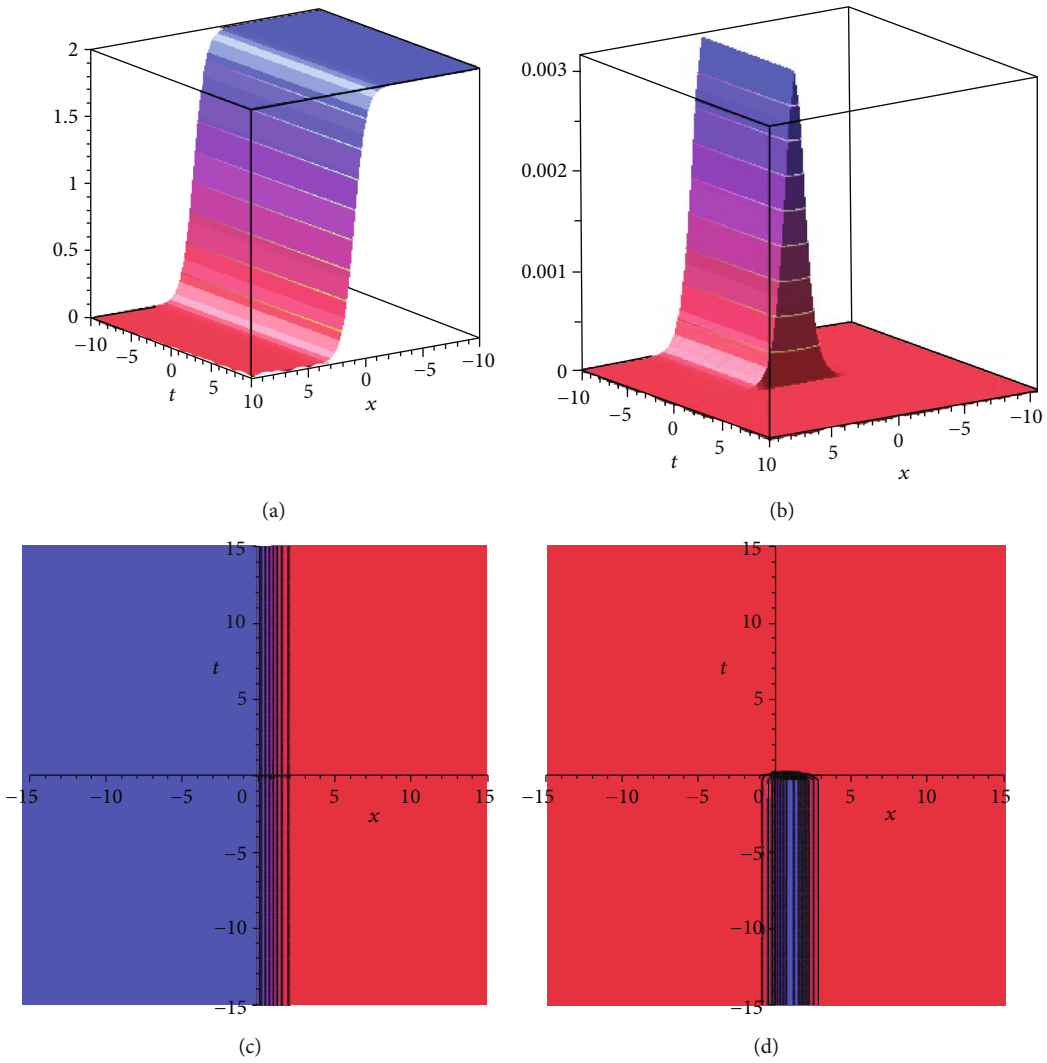

FIGURE 4: The graphical representation of the solution $\lambda_8(x,t)$: (a) real three-dimensional shape, (b) complex three-dimensional shape, (c) real contour plot, and (d) imaginary contour plot.

$$\lambda_2(x,t) = -S_1 \coth\left\{x - \frac{Vt^\beta}{\Gamma(\beta+1)}\right\}. \tag{14}$$

Cluster II:

$$V = 2S_0 - 1, S_0 = S_0, S_1 = 1, T_1 = 0. \tag{15}$$

Similarly, we get

$$\lambda_3(x,t) = S_0 - \tanh\left\{x - \frac{Vt^\beta}{\Gamma(\beta+1)}\right\}. \tag{16}$$

$$\lambda_4(x,t) = S_0 - \coth\left\{x - \frac{Vt^\beta}{\Gamma(\beta+1)}\right\}. \tag{17}$$

Cluster III:

$$V = 3, S_0 = 2, S_1 = 2, T_1 = -1. \tag{18}$$

Similarly, we get

$$\lambda_5(x,t) = 2 - \frac{1}{\tanh\left\{x - Vt^\beta/\Gamma(\beta+1)\right\}} - \tanh\left\{x - \frac{Vt^\beta}{\Gamma(\beta+1)}\right\}. \tag{19}$$

$$\lambda_6(x,t) = 2 - \frac{1}{\coth\left\{x - Vt^\beta/\Gamma(\beta+1)\right\}} - \coth\left\{x - \frac{Vt^\beta}{\Gamma(\beta+1)}\right\}. \tag{20}$$

Cluster IV:

$$V = 1, S_0 = 1, S_1 = 1, T_1 = -1. \tag{21}$$

Similarly, we get

$$\lambda_7(x,t) = 1 - \frac{1}{\tanh\left\{x - Vt^\beta/\Gamma(\beta+1)\right\}}. \tag{22}$$

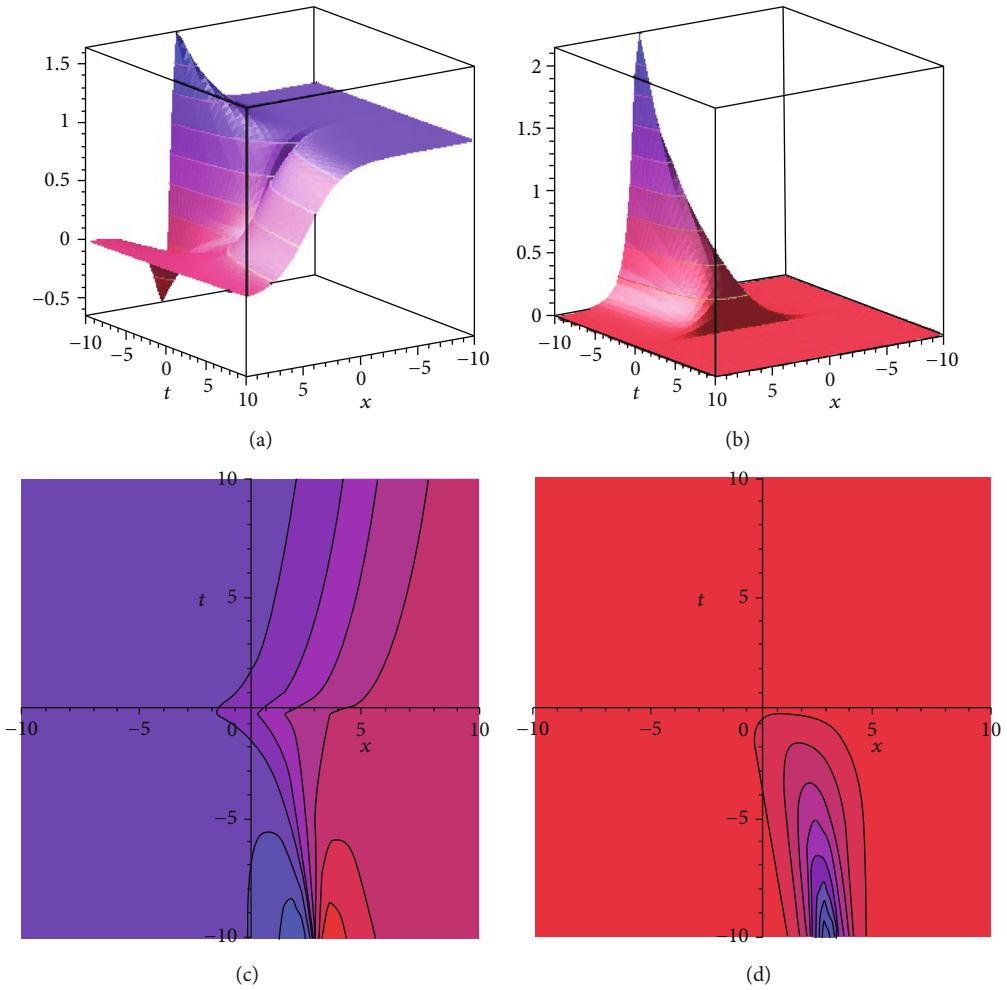

Figure 5: The graphical representation of the solution $\Phi_1(x,t)$: (a) real three-dimensional shape, (b) complex three-dimensional shape, (c) real contour plot, and (d) imaginary contour plot.

$$\lambda_8(x,t) = 1 - \frac{1}{\coth\left\{x - Vt^{\beta}/\Gamma(\beta+1)\right\}}. \tag{23}$$

3.2. Constructing the Solutions of the NFCA Equation. We are considering the NFCA equation [42].

$$D_t^{\beta}\Phi - \Phi_{xx} + \Phi^3 - \Phi = 0, t > 0, 0 < \beta \le 1. \tag{24}$$

We introduce

$$\Phi(x,t) = \Phi(\eta), \eta = kx - \frac{Vt^{\beta}}{\Gamma(\beta+1)}, \tag{25}$$

where k and V are arbitrary constants. Implementing equations (25) and (24), then, we get

$$-V\Phi' - k^2\Phi'' + \Phi^3 - \Phi = 0. \tag{26}$$

We find from equation (4). Then, we have

$$\Phi(\eta) = S_0\Psi^0 + S_1\Psi^1 + T_1\Psi^0\Phi = S_0 + \frac{T_1}{\Omega} - (S_1 + T_1)\Omega. \tag{27}$$

Collecting the coefficient of Ψ and Φ and solving the resulting system, then, we find

Cluster I:

$$V = \frac{3}{4}, k = \pm\frac{1}{2\sqrt{2}}, S_0 = \frac{1}{2}, S_1 = \frac{1}{2}, T_1 = 0. \tag{28}$$

Substituting the above values in equation (27), we get

$$\Phi_1(x,t) = \frac{1}{2}\left\{1 - \tanh\left(kx - \frac{Vt^{\beta}}{\Gamma(\beta+1)}\right)\right\}. \tag{29}$$

$$\Phi_2(x,t) = \frac{1}{2}\left\{1 - \coth\left(kx - \frac{Vt^{\beta}}{\Gamma(\beta+1)}\right)\right\}. \tag{30}$$

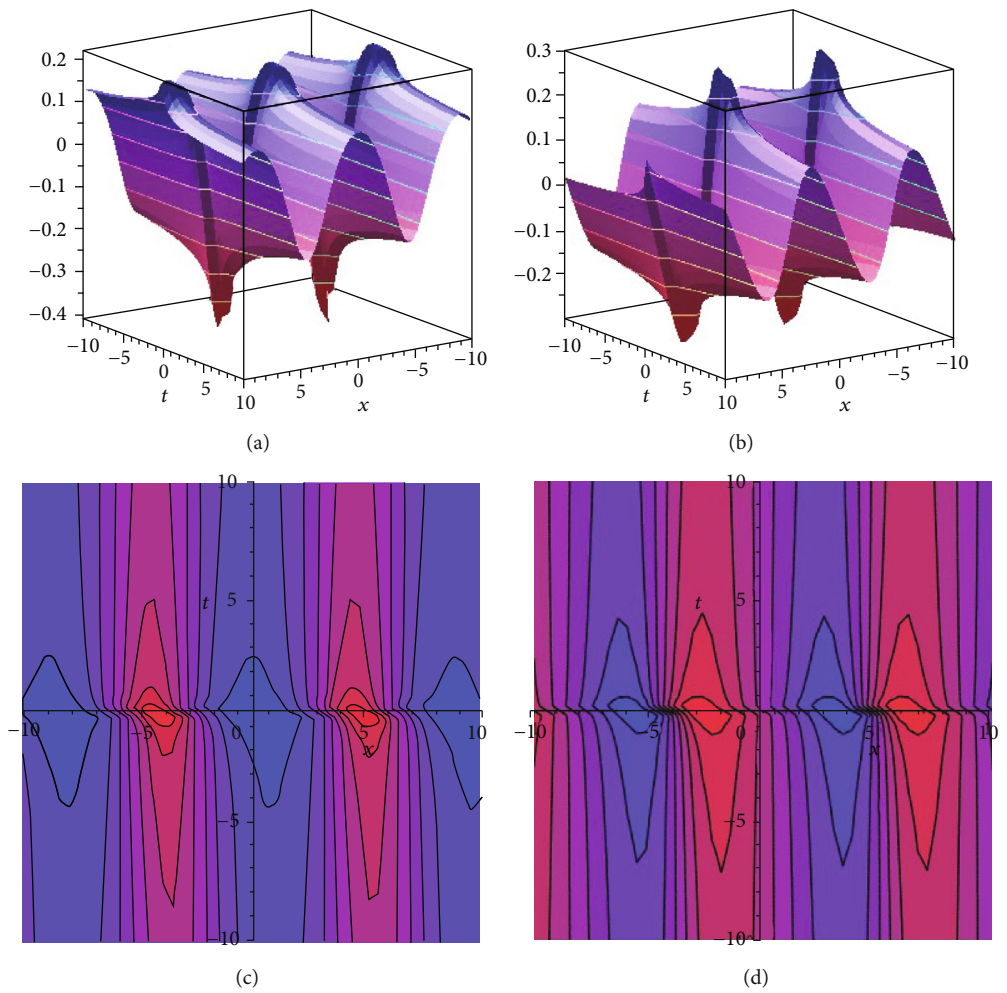

FIGURE 6: The graphical representation of the solution $\Phi_3(x,t)$: (a) real three-dimensional shape, (b) complex three-dimensional shape, (c) real contour plot, and (d) imaginary contour plot.

Cluster II:

$$V=\frac{3}{4},k=\frac{1}{2}\left(\pm\sqrt{\frac{-1}{2}}\right),S_0=\frac{1}{2},S_1=-\frac{1}{2},T_1=0. \quad (31)$$

Similarly, we get

$$\Phi_3(x,t)=\frac{1}{2}\left\{1+\tanh\left(kx-\frac{Vt^{\beta}}{\Gamma(\beta+1)}\right)\right\}. \quad (32)$$

$$\Phi_4(x,t)=\frac{1}{2}\left\{1+\coth\left(kx-\frac{Vt^{\beta}}{\Gamma(\beta+1)}\right)\right\}. \quad (33)$$

Cluster III:

$$V=\frac{3}{4},k=\frac{1}{2}\left(\pm\sqrt{\frac{-1}{2}}\right),S_0=-\frac{1}{2},S_1=\frac{1}{2},T_1=0. \quad (34)$$

Similarly, we get

$$\Phi_5(x,t)=-\frac{1}{2}\left\{1+\tanh\left(kx-\frac{Vt^{\beta}}{\Gamma(\beta+1)}\right)\right\}. \quad (35)$$

$$\Phi_6(x,t)=-\frac{1}{2}\left\{1+\coth\left(kx-\frac{Vt^{\beta}}{\Gamma(\beta+1)}\right)\right\}. \quad (36)$$

Cluster IV:

$$V=\frac{3}{4},k=\frac{1}{2}\left(\pm\sqrt{\frac{-1}{2}}\right),S_0=-\frac{1}{2},S_1=-\frac{1}{2},T_1=0. \quad (37)$$

Similarly, we get

$$\Phi_7(x,t)=-\frac{1}{2}\left\{1-\tanh\left(kx-\frac{Vt^{\beta}}{\Gamma(\beta+1)}\right)\right\}. \quad (38)$$

$$\Phi_8(x,t)=-\frac{1}{2}\left\{1-\coth\left(kx-\frac{Vt^{\beta}}{\Gamma(\beta+1)}\right)\right\}. \quad (39)$$

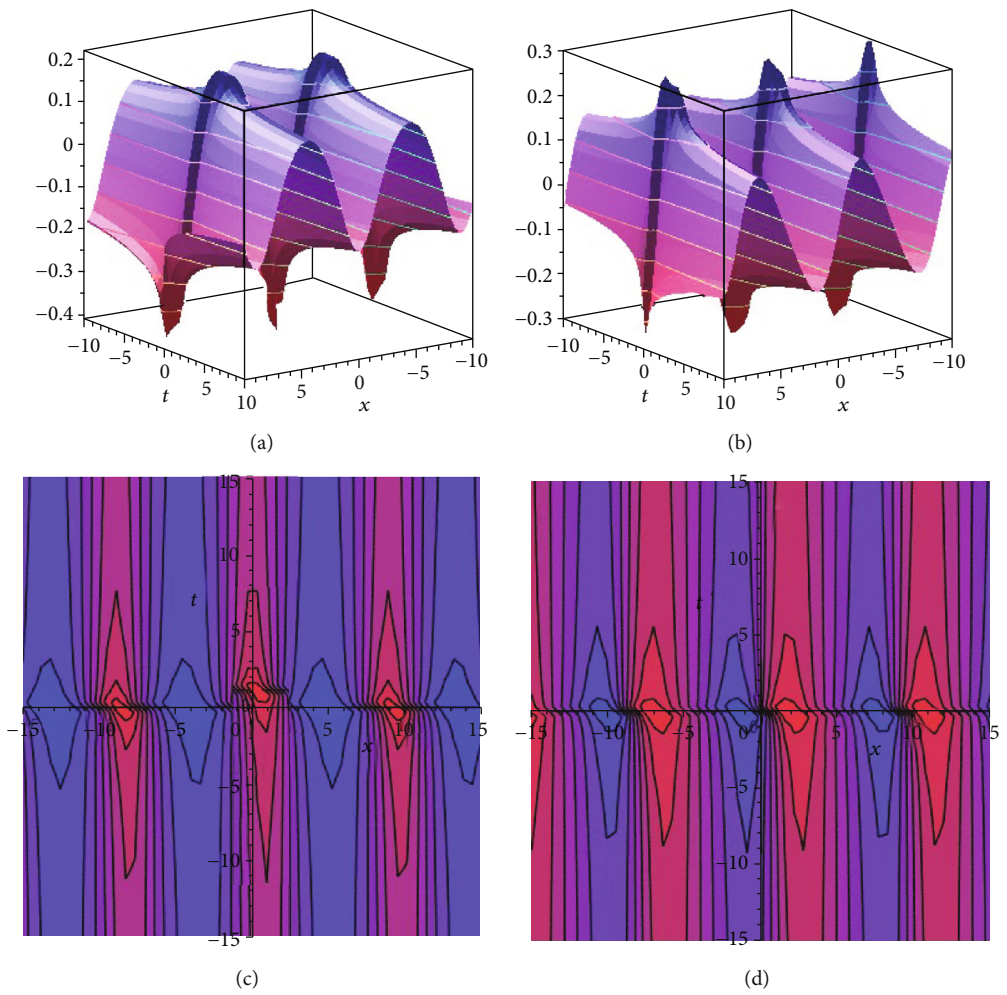

Figure 7: The graphical representation of the solution $\Phi_4(x,t)$: (a) real three-dimensional shape, (b) complex three-dimensional shape, (c) real contour plot, and (d) imaginary contour plot.

Cluster V:

$$V=\frac{3}{4},k=\frac{1}{2}\left(\pm\sqrt{\frac{1}{2}}\right),S_0=-\frac{1}{2},S_1=-\frac{1}{2},T_1=\frac{1}{2}. \quad (40)$$

Similarly, we get

$$\Phi_9(x,t)=-\frac{1}{2}\left\{1-\frac{1}{\tanh\left(kx-Vt^{\beta}/\Gamma(\beta+1)\right)}\right\}. \quad (41)$$

$$\Phi_{10}(x,t)=-\frac{1}{2}\left\{1-\frac{1}{\coth\left(kx-Vt^{\beta}/\Gamma(\beta+1)\right)}\right\}. \quad (42)$$

Cluster VI:

$$V=\frac{3}{4},k=\frac{1}{2}\left(\pm\sqrt{\frac{1}{2}}\right),S_0=\frac{1}{2},S_1=\frac{1}{2},T_1=-\frac{1}{2}. \quad (43)$$

Similarly, we get

$$\Phi_{11}(x,t)=\frac{1}{2}\left\{1-\frac{1}{\tanh\left(kx-Vt^{\beta}/\Gamma(\beta+1)\right)}\right\}. \quad (44)$$

$$\Phi_{12}(x,t)=\frac{1}{2}\left\{1-\frac{1}{\coth\left(kx-Vt^{\beta}/\Gamma(\beta+1)\right)}\right\}. \quad (45)$$

Cluster VII:

$$V=\frac{3}{8},k=\frac{1}{4}\left(\pm\sqrt{\frac{1}{2}}\right),S_0=-\frac{1}{2},S_1=-\frac{1}{2},T_1=\frac{1}{4}. \quad (46)$$

Similarly, we get:

$$\Phi_{13}(x,t)=-\frac{1}{2}+\frac{1}{4\tanh\left\{kx-Vt^{\beta}/\Gamma(\beta+1)\right\}}+\tanh\left\{kx-\frac{Vt^{\beta}}{\Gamma(\beta+1)}\right\}. \quad (47)$$

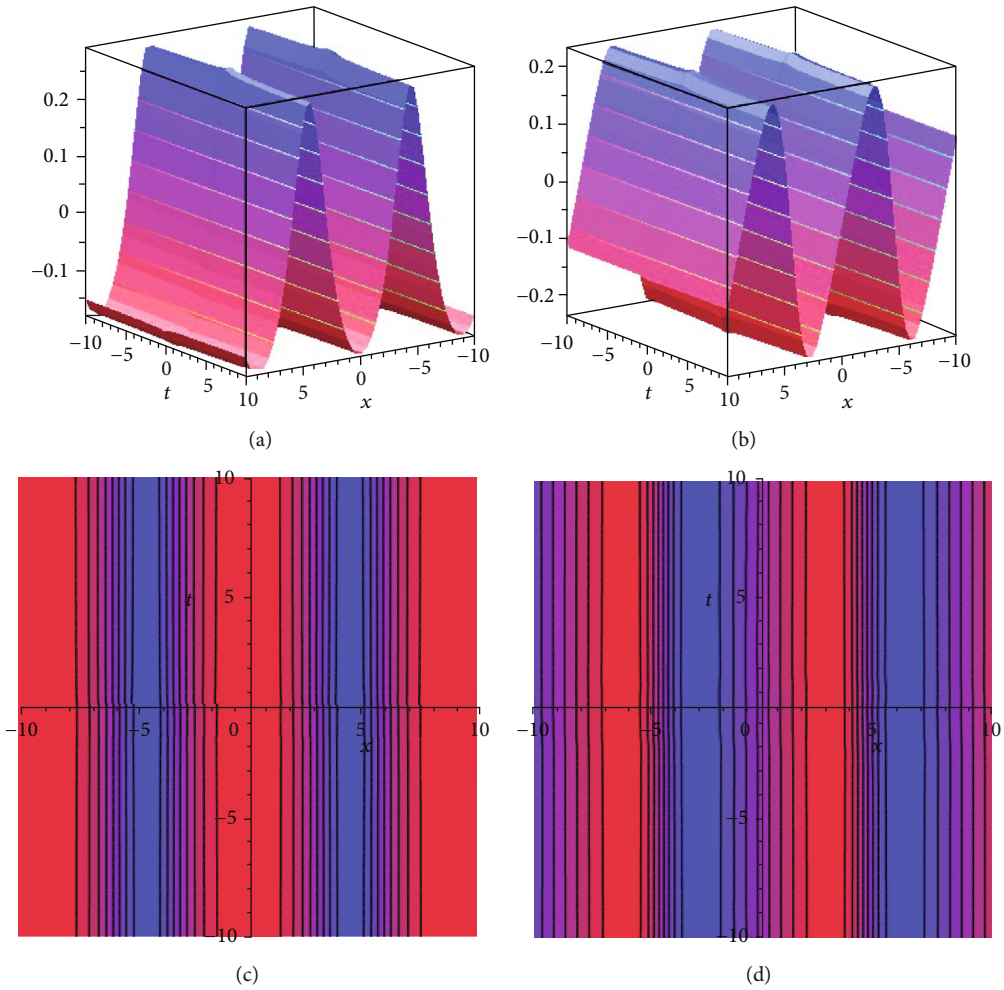

FIGURE 8: The graphical representation of the solution $\Phi_5(x,t)$: (a) real three-dimensional shape, (b) complex three-dimensional shape, (c) real contour plot, and (d) imaginary contour plot.

$$\Phi_{14}(x,t) = -\frac{1}{2} + \frac{1}{4\coth\left\{kx - Vt^{\beta}/\Gamma(\beta+1)\right\}} + \coth\left\{kx - \frac{Vt^{\beta}}{\Gamma(\beta+1)}\right\}. \tag{48}$$

Cluster VIII:

$$V = \frac{3}{8}, k = \frac{1}{4}\left(\pm\sqrt{\frac{1}{2}}\right), S_0 = \frac{1}{2}, S_1 = \frac{1}{2}, T_1 = -\frac{1}{4}. \tag{49}$$

Similarly, we get:

$$\Phi_{15}(x,t) = \frac{1}{2} - \frac{1}{4\tanh\left\{kx - Vt^{\beta}/\Gamma(\beta+1)\right\}} - \frac{1}{4}\tanh\left\{kx - \frac{Vt^{\beta}}{\Gamma(\beta+1)}\right\}. \tag{50}$$

$$\Phi_{16}(x,t) = \frac{1}{2} - \frac{1}{4\coth\left\{kx - Vt^{\beta}/\Gamma(\beta+1)\right\}} - \frac{1}{4}\coth\left\{kx - \frac{Vt^{\beta}}{\Gamma(\beta+1)}\right\}. \tag{51}$$

4. Numerical Simulations

Shehata and Amra [34] have offered a process named the variation of $(G^{'}/G)$-extension approach to look for the studied equation's exact structures and achieve many results shown in Section 3. Comparison between other methods, the studied approach is provided a more exact answer rather than the other approach. On the additional support, the auxiliary model employed in the integral method is different, and so the exact structures obtained are also other. Likewise, for any fractional nonlinear models, it could be determined that the studied approach is extremely more straightforward than the other schemes. In this paper, the integrable method applies to the studied fractional nonlinear models for the first time. We confirm that any other authors did not use the technique on the studied fractional nonlinear models. This part also will present numerous types of soliton of the created answers for various values of the constant coefficients. The kinds of the solitons are kink type soliton profiles, singular kink type soliton profiles, periodic wave soliton profiles, and so many. Also, we provide the contour graph of the attained answers which is constructed commencing binary variable tasks. One variable exemplifies on the horizontal axis and a second variable

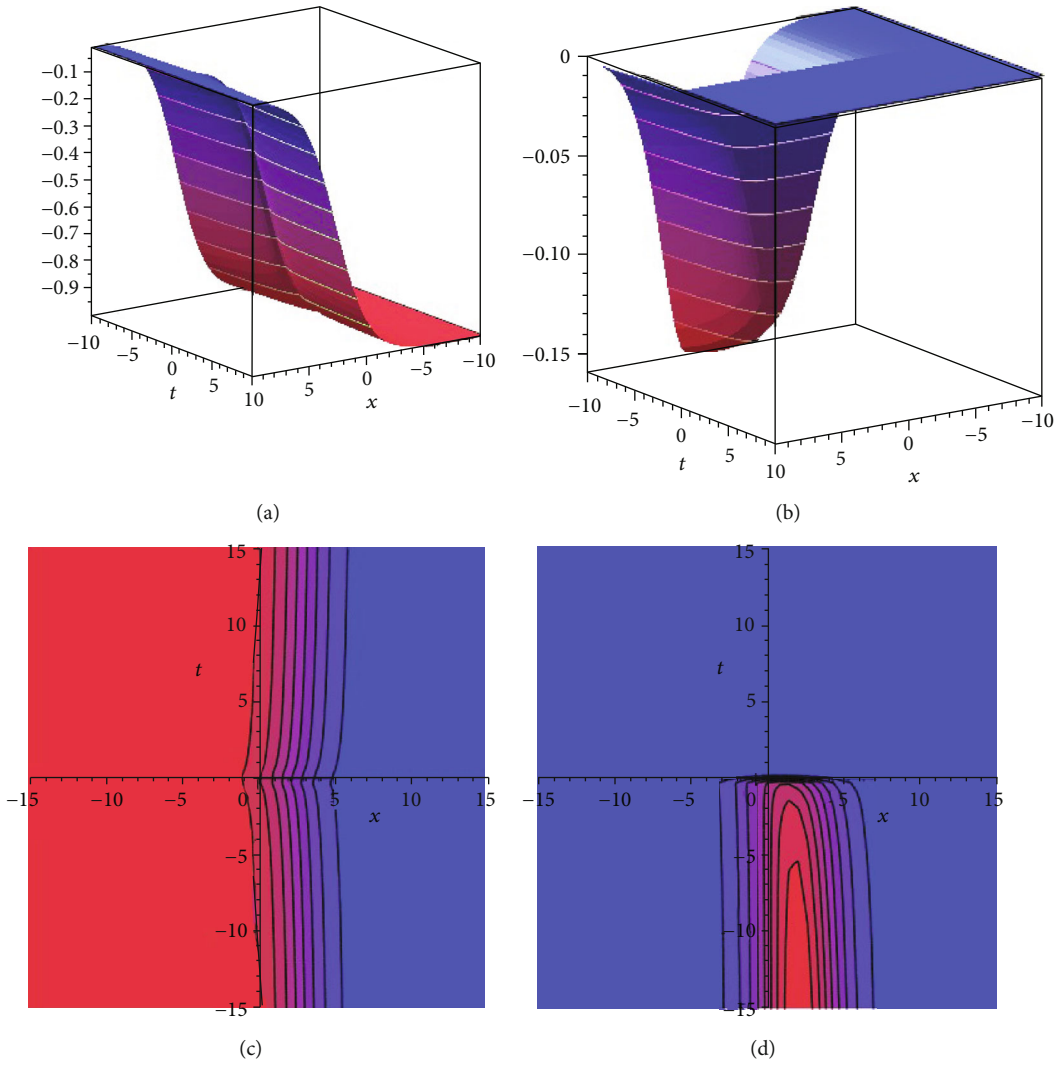

Figure 9: The graphical representation of the solution $\Phi_{10}(x,t)$: (a) real three-dimensional shape, (b) complex three-dimensional shape, (c) real contour plot, and (d) imaginary contour plot.

exemplifies on the vertical axis. The functional value exemplifies the color gradient and isolines. Contour graphs are technique to expression a 3D surface on a 2D plane. This kind of graph is broadly implemented in applied mathematics, mathematical physics, and engineering, where the contour lines normally demonstration elevation.

4.1. Graphical Representations of the Solution to the FCRWP Equation. In the current section, we have offered numerous mathematical simulations through the proposed procedure. To explain the dynamic performances of the answers acquired in Section 3.1. Figures 1–4 illustrate the graphical depictions of some selected computational results of the problem received utilizing the studied method. They are pictured below.

Figure 1 demonstrates the dynamic performance of $\lambda_1(x,t)$ using $\alpha = 0.5$. In particular, Figure 1 demonstrates the 3D shape and contour shape of $\lambda_1(x,t)$. This shape represents intersection between rough wave and kinky soliton wave profiles. The solution attributes of $\lambda_3(x,t)$ are displayed in Figure 2 using $\alpha = 0.9$. This shape represents intersection between lump wave and kinky soliton wave profiles. In Figure 3, we demonstrate the dynamic performance of $\lambda_6(x,t)$ using $\alpha = 0.01$. In particular, Figure 3 shows the three-dimensional shape and contour shape of the solution $\lambda_6(x,t)$. This shape represents soliton wave profiles. Figure 4 demonstrates the dynamic performances of $\lambda_8(x,t)$ by taking $\alpha = 0.001$. In particular, Figure 4 shows the three-dimensional shape and contour shape of the solution $\lambda_8(x,t)$. This shape represents kink wave profiles. The implemented mathematical simulations acknowledge that the answers are of periodic wave shapes and the rational, hyperbolic, trigonometric categorizations. Furthermore, through wisely observing at the construction of the acquired answers, it could be comprehended that the connecting fractional derivatives parameter of β performs in the formulation of all the answers.

4.2. Graphical Representations of the Solution to the NFCA Equation. In the current section, we have implemented numerous mathematical simulations through the proposed process. To explain the dynamic performances of the

answers acquired in Section 3.2. Figures 5–9 illustrate the graphical depictions of some selected computational results of the problem received utilizing the studied method. They are pictured below.

Figure 5 demonstrates the dynamic performance of $\Phi_1(x,t)$ using $\alpha = 0.3$. In particular, Figure 5 demonstrates the 3D figure and contour figure of $\Phi_1(x,t)$. This shape represents intersection between lump wave and kinky soliton wave profiles. The solution attributes of $\Phi_3(x,t)$ are displayed in Figure 6 using $\alpha = 0.1$. Figure 6 demonstrates the 3D figure and contour figure of $\Phi_3(x,t)$. This shape represents intersection between rough wave and periodic wave profiles. In Figure 7, we demonstrate the dynamic performance of $\Phi_4(x,t)$ using $\alpha = 0.1$. In particular, Figure 7 demonstrates the three-dimensional shape and contour shape of the solution $\Phi_4(x,t)$. This shape represents intersection between lump wave and periodic wave profiles. Figure 8 demonstrates the dynamic performances of $\Phi_5(x,t)$ by taking $\alpha = 0.005$. In particular, Figure 8 shows the three-dimensional shape and contour shape of the solution $\Phi_5(x,t)$. This shape represents periodic wave profiles. Finally, we demonstrate singular kink wave profiles of the solution $\Phi_{10}(x,t)$ by taking $\alpha = 0.1$ which is displayed in Figure 9. The implemented mathematical simulations acknowledge that the answers are of periodic wave shapes and the rational, hyperbolic, trigonometric categorizations. Furthermore, through wisely observing at the construction of the acquired answers, it could be comprehended that the connecting fractional derivative parameter of β performs in the formulation of all the answers.

5. Conclusion

In the current research, we successfully implement the studied technique to demonstration that this scheme is well-organized and virtually fine well-matched to implement in getting answers for FCRWP equation and the NFCA equation. The various of dynamical behaviors such as intersection between rough wave and kinky soliton wave profiles, intersection between lump wave and kinky soliton wave profiles, soliton wave profiles, kink wave profiles, intersection between lump wave and periodic wave profiles, intersection between rough wave and periodic wave profiles, periodic wave profiles, and kink wave profiles are taken in the present study which present in well-defined regions of mathematical physics. These solutions will be useful for further studies in mathematical physics which are shown in Figures 1–9.

In Figure 1, we represent intersection between rough wave and kinky soliton wave profiles. Figure 2 represents intersection between lump wave and kinky soliton wave profiles. Figure 3 shows soliton wave profiles. Figure 4 shows kink wave profiles. Figure 5 demonstrates intersection between lump wave and kinky soliton wave profiles. Figure 6 demonstrates intersection between rough wave and periodic wave profiles. In Figure 7, we demonstrate intersection between lump wave and periodic wave profiles. Figure 8 demonstrates periodic wave profiles. Finally, we demonstrate singular kink wave profiles which are displayed in Figure 9. The most powerful aspect of this method is that it can be applied to other fractional nonlinear models. Also, it has observed that the results obtained in this study have been presented for the first time. It is important to note that the solutions obtained can be applied to nonlinear models, plasma physics, optical physics, ion-acoustics physics, optical engineering, soliton theory, nonlinear dynamics, and other areas.

Data Availability

The data used to support the findings of this study are included within the article.

Conflicts of Interest

The authors declare that they have no conflicts of interest.

References

[1] M. N. Alam, A. R. Seadawy, and D. Baleanu, "Closed-form wave structures of the space-time fractional Hirota–Satsuma coupled KdV equation with nonlinear physical phenomena," *Open Physics*, vol. 18, no. 1, pp. 555–565, 2020.

[2] M. N. Alam, S. Aktar, and C. Tunc, "New solitary wave structures to time fractional biological population model," *Journal of Mathematical Analysis-JMA*, vol. 11, no. 3, pp. 59–70, 2020.

[3] M. N. Alam and C. Tunc, "The new solitary wave structures for the (2 + 1)-dimensional time-fractional Schrodinger equation and the space-time nonlinear conformable fractional Bogoyavlenskii equations," *Alexandria Engineering Journal*, vol. 59, no. 4, pp. 2221–2232, 2020.

[4] M. N. Alam and X. Li, "New soliton solutions to the nonlinear complex fractional Schrödinger equation and the conformable time-fractional Klein–Gordon equation with quadratic and cubic nonlinearity," *Physica Scripta*, vol. 95, no. 4, p. 045224, 2020.

[5] M. N. Alam, A. R. Seadawy, and D. Baleanu, "Closed-form solutions to the solitary wave equation in an unmagnatized dusty plasma," *Alexandria Engineering Journal*, vol. 59, no. 3, pp. 1505–1514, 2020.

[6] H. Yepez-Martınez, J. F. Gomez-Aguilar, and A. Atangana, "First integral method for non-linear differential equations with conformable derivative," *Mathematical Modelling of Natural Phenomena*, vol. 13, no. 1, p. 14, 2018.

[7] Y. Gurefe, "The generalized Kudryashov method for the nonlinear fractional partial differential equations with the beta-derivative," *Revista Mexicana de Fısica*, vol. 66, no. 6 Nov-Dec, pp. 771–781, 2020.

[8] H. Yepez-Martınez and J. F. Gomez-Aguilar, "Fractional sub-equation method for Hirota-Satsuma-coupled KdV equation and coupled mKdV equation using the Atangana's conformable derivative," *Waves in Random and Complex Media*, vol. 29, no. 4, pp. 678–693, 2019.

[9] S. Zhang and H. Q. Zhang, "Fractional sub-equation method and its applications to nonlinear fractional PDEs," *Physics Letters A*, vol. 375, no. 7, pp. 1069–1073, 2011.

[10] J. Jiang, Y. Feng, and S. Li, "Improved fractional subequation method and exact solutions to fractional partial differential equations," vol. 2020, Article ID 5840920, 18 pages, 2020.

[11] B. Ghanbari and D. Baleanu, "New optical solutions of the fractional Gerdjikov-Ivanov equation with conformable derivative," *Frontiers of Physics*, vol. 8, p. 167, 2020.

[12] A. Tozar, A. Kurt, and O. Tasbozan, "New wave solutions of time fractional integrable dispersive wave equation arising in ocean engineering models," *Kuwait Journal of Science*, vol. 47, no. 2, pp. 22–33, 2020.

[13] A. Korkmaz, O. E. Hepson, K. Hosseini, H. Rezazadeh, and M. Eslami, "Sine-Gordon expansion method for exact solutions to conformable time fractional equations in RLW-class," *Journal of King Saud University–Science*, vol. 32, no. 1, 2018.

[14] H. Aminikhah, A. H. Refahi Sheikhani, and H. Rezazadeh, "Sub-equation method for the fractional regularized long-wave equations with conformable fractional derivatives," *Scientia Iranica*, vol. 23, no. 3, pp. 1048–1054, 2016.

[15] K. Hosseini, M. Mirzazadeh, M. Ilie, and S. Radmehr, "Dynamics of optical solitons in the perturbed Gerdjikov-Ivanov equation," *Optik*, vol. 206, p. 164350, 2020.

[16] K. Hosseini, M. Mirzazadeh, J. Vahidi, and R. Asghari, "Optical wave structures to the Fokas-Lenells equation," *Optik*, vol. 207, p. 164450, 2020.

[17] K. Hosseini, M. Mirzazadeh, F. Rabiei, H. M. Baskonus, and G. Yel, "Dark optical solitons to the Biswas-Arshed equation with high order dispersions and absence of the self-phase modulation," *Optik*, vol. 209, p. 164576, 2020.

[18] E. C. Aslan and M. Inc, "Optical soliton solutions of the NLSE with quadratic-cubic-hamiltonian perturbations and modulation instability analysis," *Optik*, vol. 196, p. 162661, 2019.

[19] G. M. Ismail, H. R. A. Rahim, A. A. Aty, R. Kharabsheh, W. Alharbi, and M. A. Aty, "An analytical solution for fractional oscillator in a resisting medium," *Chaos, Solitons & Fractals*, vol. 130, p. 109395, 2020.

[20] H. Ahmad, A. Akgül, T. A. Khan, P. S. Stanimirović, and Y. M. Chu, "A new analyzing technique for nonlinear time fractional Cauchy reaction- diffusion model equations," *Results in Physics*, vol. 19, p. 103462, 2020.

[21] H. Ahmad, A. Akgül, T. A. Khan, P. S. Stanimirović, and Y. M. Chu, "New perspective on the conventional solutions of the nonlinear time-fractional partial differential equations," *Complexity*, vol. 2020, Article ID 8829017, 10 pages, 2020.

[22] M. S. Osman, H. Rezazadeh, and M. Eslami, "Traveling wave solutions for (3+1) dimensional conformable fractional Zakharov-Kuznetsov equation with power law nonlinearity," *Nonlinear Engineering*, vol. 8, no. 1, pp. 559–567, 2019.

[23] C. Park, R. I. Nuruddeen, K. K. Ali, L. Muhammad, M. S. Osman, and D. Baleanu, "Novel hyperbolic and exponential ansatz methods to the fractional fifth-order Korteweg de Vries equations," *Adv. Difference Equ.*, vol. 2020, no. 1, p. 627, 2020.

[24] I. Siddique, M. M. M. Jaradat, A. Zafar, K. B. Mehdi, and M. S. Osman, "Exact traveling wave solutions for two prolific conformable M-fractional differential equations via three diverse approaches," *Results in Physics*, vol. 28, p. 104557, 2021.

[25] A. Khalid, A. Rehan, K. S. Nisar, and M. S. Osman, "Splines solutions of boundary value problems that arises in sculpturing electrical process of motors with two rotating mechanism circuit," *Physica Scripta*, vol. 96, no. 10, p. 104001, 2021.

[26] C. Yue, A. Elmoasry, M. M. A. Khater et al., "On complex wave structures related to the nonlinear long–short wave interaction system: analytical and numerical techniques," *AIP Advances*, vol. 10, no. 4, p. 045212, 2020.

[27] O. A. Arqub, M. A. Smadi, H. Almusawa et al., "A novel analytical algorithm for generalized fifth-order time-fractional nonlinear evolution equations with conformable time derivative arising in shallow water waves," *Alexandria Engineering Journal*, vol. 61, no. 7, pp. 5753–5769, 2022.

[28] S. Tarla, K. K. Ali, T. C. Sun, R. Yilmazer, and M. S. Osman, "Nonlinear pulse propagation for novel optical solitons modeled by Fokas system in monomode optical fibers," *Results in Physics*, vol. 36, p. 105381, 2022.

[29] S. Kumar, S. K. Dhiman, D. Baleanu, M. S. Osman, and A. M. Wazwaz, "Lie symmetries, closed-form solutions, and various dynamical profiles of solitons for the variable coefficient (2+1)-dimensional KP equations," *Symmetry*, vol. 14, no. 3, p. 597, 2022.

[30] K. K. Ali, R. Yilmazer, and M. S. Osman, "Dynamic behavior of the (3+1)-dimensional KdV–Calogero–Bogoyavlenskii–Schiff equation," *Optical and Quantum Electronics*, vol. 54, no. 3, p. 160, 2022.

[31] J. G. Liu, W. H. Zhu, M. S. Osman, and W. X. Ma, "An explicit plethora of different classes of interactive lump solutions for an extension form of 3D-Jimbo-Miwa model," *The European Physical Journal - Plus*, vol. 135, no. 5, p. 412, 2020.

[32] A. Zafar, M. Raheel, M. Q. Zafar et al., "Dynamics of different nonlinearities to the perturbed nonlinear Schrödinger equation via solitary wave solutions with numerical simulation," *Fractal and Fractional*, vol. 5, no. 4, p. 213, 2021.

[33] B. Inan, M. S. Osman, T. Ak, and D. Baleanu, "Analytical and numerical solutions of mathematical biology models: the Newell- Whitehead-Segel and Allen-Cahn equations," *Mathematical Methods in the Applied Sciences*, vol. 43, no. 5, pp. 2588–2600, 2020.

[34] A. R. Shehata and S. S. M. Abu-Amra, "Geometrical properties and exact solutions of three (3 + 1)-dimensional nonlinear evolution equations in mathematical physics using different expansion methods," *Journal of Advances in Mathematics and Computer Science*, vol. 33, pp. 1–19, 2019.

[35] K. S. Miller and B. Ross, *An Introduction to the fractional calculus and fractional differential equations*, Wiley, New York, 1993.

[36] A. A. Kilbas, H. M. Srivastava, and J. J. Trujillo, *Theory and Applications of Fractional Differential Equations*, Elsevier, San Diego, 2006.

[37] I. Podlubny, *Fractional Differential Equations*, Academic Press, San Diego, 1999.

[38] G. Jumarie, "Modified Riemann-Liouville derivative and fractional Taylor series of nondifferentiable functions further results," *Computers & Mathematcs with Applications*, vol. 51, no. 9-10, pp. 1367–1376, 2006.

[39] G. Jumarie, "Table of some basic fractional calculus formulae derived from a modified Riemann-Liouville derivative for non-differentiable functions," *Applied Mathematics Letters*, vol. 22, no. 3, pp. 378–385, 2009.

[40] Z. Ganji, D. Ganji, A. D. Ganji, and M. Rostamian, "Analytical solution of time-fractional Navier–Stokes equation in polar coordinate by homotopy perturbation method," *Numerical Methods for Partial Differential Equations*, vol. 26, no. 1, pp. 117–124, 2010.

[41] O. Gunera, A. Bekir, and Ö. Ünsal, "Two reliable methods for solving the time fractional clannish random Walker's parabolic equation," *Optik*, vol. 127, no. 20, pp. 9571–9577, 2016.

[42] S. Javeed, S. Saif, and D. Baleanu, "New exact solutions of fractional Cahn-Allen equation and fractional DSW system," *Adv. Difference Equ.*, vol. 2018, no. 1, p. 459, 2018.